A novel modular device for biological impedance measurements: The differential impedimetric sensor cell (DISC)

Peter Cornelis[*,1], Gideon Wackers[1], Isabelle Thomas[2], Max Brand[2], Tristan Putzeys[1,3], Alessia Gennaro[1], Michael Wübbenhorst[1], Sven Ingebrandt[2] and Patrick Wagner[1]

[1] KULeuven, Department of Physics and Astronomy, Soft-Matter Physics and Biophysics Section (ZMB), Celestijnenlaan 200 D, 3001 Leuven, Belgium
[2] University of Applied Sciences Kaiserslautern, Department of Informatics and Microsystem Technology, Amerikastr. 1, 66482 Zweibrücken, Germany
[3] KULeuven, Department of Neurosciences, Research Group Experimental Oto-Rhino-Laryngology (ExpORL), O&N II Herestraat 49, 3000 Leuven, Belgium

Received ZZZ, revised ZZZ, accepted ZZZ
Published online ZZZ (Dates will be provided by the publisher.)

Keywords Biosensor, Electrochemical Impedance Spectroscopy, Impedance-based Biosensor, Label-free detection.

For medical diagnostics, food-safety analysis and detection of environmental pollutants, simultaneous detection and quantification of multiple target molecules would be a great advantage. Impedimetric measurements using molecularly imprinted polymers (MIPs), antibodies or aptamers as biomimetic sensors are becoming a well-established technique for detecting, quantifying and analysing various biological targets such as DNA, proteins and small molecules. The most commonly implemented systems use non-Faradaic impedance spectroscopy. Adding a redox probe such as silver/silver chloride allows for the use of Faradaic impedance spectroscopy techniques using redox-active molecules such as ferricyanide thereby extending the range of possible applications. Furthermore, the ability to perform differential measurements would allow the use of undiluted patient samples which significantly simplifies sample preparation. Therefore, adapting this low-cost technique to simultaneously perform differential measurements on multiple targets and making it easy to use has great potential in a wide range of applications. In this work, a system that meets these requirements has been successfully designed and fabricated. Up to eight different targets can be quasi-simultaneously analysed. Furthermore, the system was validated against a high-resolution dielectric spectrometer (Novocontrol, Alpha analyser) using well characterised samples at different temperatures over the whole frequency range (10 Hz – 100 kHz).

The DISC (left) houses the flowcell and all sensor electrodes while the electronic base unit (EBU) (right) contains all the control electronics. Dividing the system into these two modules allows for easy cleaning and sterilization because all the sensitive electronics are in a separate module that does not require sterilization.

1 Introduction

Impedimetric measurements using biosensors are becoming well-established as evidenced in multiple review articles [1-4]. This technique has a broad variety of applications as the following examples may demonstrate: DNA detection and analysis [5-7], monitoring cell viability using interdigitated electrodes [8], characterizing self-assembled monolayers [9] and detecting and quantifying proteins using sensors functionalized with antibodies [10] or aptamers [11]. Furthermore, even small molecules can be detected and quantified in the nano molar range using

* Corresponding author: e-mail peter.cornelis@kuleuven.be, Phone: +32 16 37 29 62

antibodies [12] or molecularly imprinted polymers (MIPS) [13-15]. Performing differential measurements, where the response of a functionalized and a non-functionalized (reference) sensor are compared, allows analysis of undiluted patient samples. Ideally, both measurements should be done simultaneously on the same sample. Impedimetric measurement techniques are also widely used in medical applications such as body fluid volume measurements and tracking of changes in the body cell mass [16-18]. For medical, food-safety and environmental applications, simultaneous measurement of multiple target molecules would be a great advantage. For instance, the presence of cadaverine dramatically increases the toxicity of histamine found in spoiled food [19, 20]. All the previously mentioned applications use non-Faradaic impedance spectroscopy which does not use redox probes. Faradaic impedance spectroscopy allows measurement of redox-active molecules by using a (pseudo) reference electrode in addition to the standard working and counter electrode [21, 22]. This technique has even lower detection limits, below 1 nM, but requires the use of auxiliary chemicals [21]. The novel modular device that was developed in this work enables up to 8 measurement channels in any combination of functionalized and non-functionalized biosensor chips. Moreover, both non-Faradaic and Faradaic impedance spectroscopy techniques can be employed.

2 Materials & Fabrication The device consists of two main subassemblies. The "Differential impedimetric sensor cell" and its controller, the "Electronic base unit" or respectively DISC and EBU for short. Polyether ether ketone (PEEK) has been used to fabricate several of the components inside the DISC. This material is thermally and chemically stabile and, most importantly, easily sterilisable.

2.1 DISC The core component is the flowcell shown in **Figure 1**. The fluid compartment has an internal volume of 310 µl. At its centre, traversing the entire cell, a gold wire is attached as the primary counter electrode for the impedance measurements. Also, two small ports are present respectively at the bottom and the top allowing an easy exchange of fluids. To counteract the formation of air bubbles, concave recesses at the inlet and outlet of the flowcell are used as transitional structures. Liquid is injected at the bottom and leaves at the top. A thermocouple is present in the bottom recess to monitor the liquid temperature.

Two chip-holder modules, each containing a sensor chip, are positioned on the left and right side of the flowcell. For this, two different module versions have been designed (**Figure 2**): A basic module, for single channel sensors with an active surface area that covers the entire area exposed to the flowcell, and an advanced module that can accommodate 1- to 4-channel sensors for which the active surface area is distributed among the required number of channels. Each module version incorporates a viton® O-ring for a perfect leak-free seal with the flowcell.

The complete measuring unit incorporates two of these modules (**Figure 3**). A large screw is used to achieve a good seal by fastening the O-ring between the flowcell and the modules and allows also for a fine-grained control over the distance between the sensor chips in the modules and the gold wire in the flowcell thanks to the compressibility of the O-ring. The vertical placement of the electrodes inside the modules has the advantage that larger particles inside complex samples cannot sediment onto their surface.

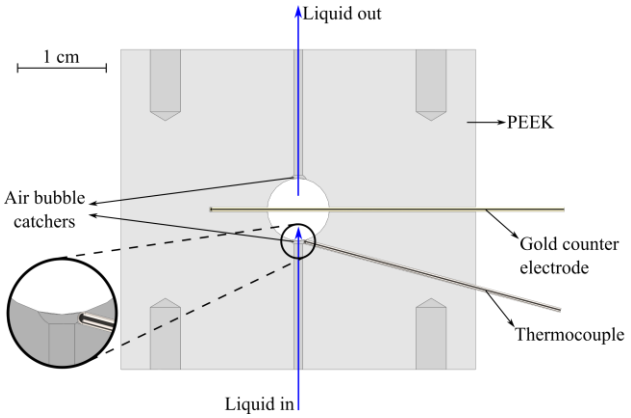

Figure 1 Schematic illustration of the flowcell. The gold counter electrode is used for impedance measurements while the thermocouple is used to monitor the temperature of the liquid. Where the liquid enters/leaves the flowcell concave recesses are present to capture and remove air bubbles from the system.

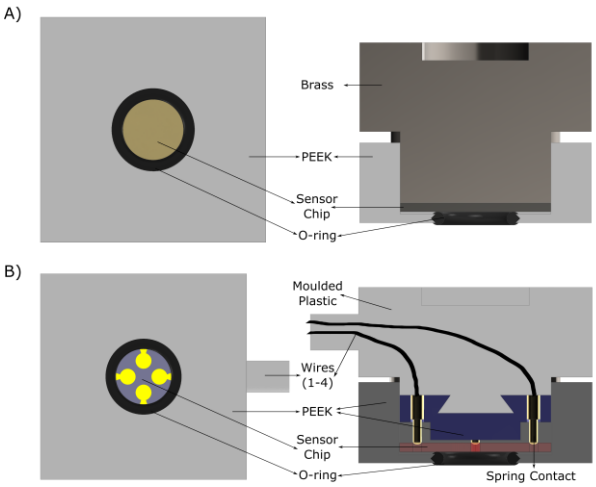

Figure 2 Schematic illustration and cross-section of the basic (A) and advanced (B) chip-holder module. The basic module uses the whole sensor chip as the measurement (working) electrode while in the advanced module spring-loaded contacts are used to connect up to four separate working electrodes on a single sensor chip.

The impedance of an electrolyte depends on its temperature and measurement frequency [23]. Therefore, a stable and tightly controlled temperature is very important for impedimetric measurements where the sensor needs to detect a change in impedance caused by the presence of its biomolecular targets. Two large heater elements, one below and one on top of the flowcell, not only allow precise control

over the temperature of the flowcell but also the injected liquid by routing the injection tubing through the bottom heater element as shown in **Figure 3**. Each heater consists of four 10 Ω power resistors in series encased in an aluminium block, which has a suitably placed hole for a thermocouple to monitor its temperature. A small T-junction can be placed at the back of the top heating element allowing a silver/silver chloride redox probe to be inserted into the outgoing liquid stream as a (pseudo) reference electrode for use in Faradaic impedance measurements [24]. Finally, to minimize the influence of electro-magnetic noise and thermal convection effects caused by air turbulence that may be present in the environment, the whole measurement unit is located inside an aluminium box with a lid for easy access as shown in **Figure 4**.

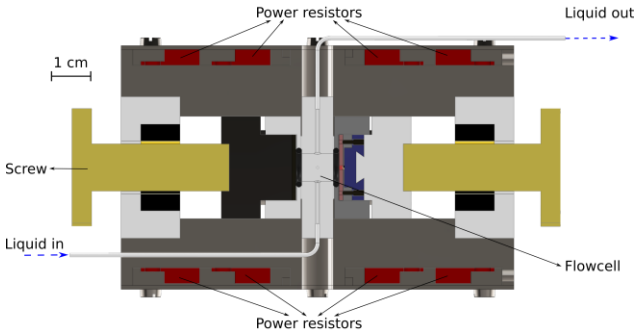

Figure 3 Schematic illustration of a cross section through the temperature controlled measurement unit. Power resistors are used for a homogeneous temperature distribution and pre-heating the incoming liquid. The screws allow fine tuning the distance between the sensor chips and the gold counter electrode.

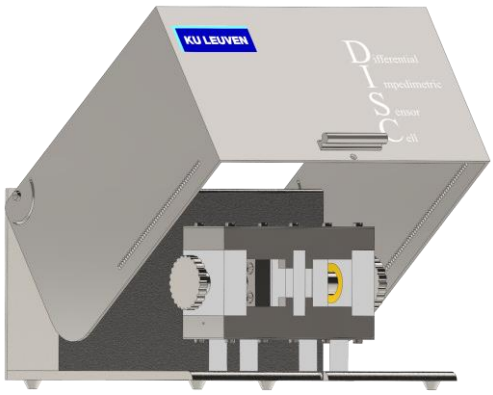

Figure 4 Schematic illustration of the DISC. The metal cover provides a stable thermal environment while also acting as a Faraday cage to reduce electro-magnetic noise from the environment.

During measurements, this box acts as a Faraday cage reducing the electro-magnetic noise and the small holes at the bottom of the lid allow for a slow non-turbulent airflow and therefore heat exchange with the environment ensuring proper operation of the heater elements. All electrical, thermocouple and liquid tubing (Teflon, 1 mm outside ⌀, 0.5 mm inside ⌀) connections were built into a panel at the back of the box for ease of use. This also ensures a clear separation between the liquid and the electronics to minimize the risk of short-circuits within the system.

2.2 Electronic Base Unit (EBU) Similarly to the DISC this is a mainly custom-made device. It is connected via USB to a computer running an in-house written LabView program which already does a basic pre-processing of the measurement data allowing easier analysis of the data at a later stage. The program also includes PID (proportional–integral–derivative) based temperature-controllers for the heater elements of the DISC to keep them at a constant temperature. Moreover, it provides an easy to navigate user-interface to set up and run experiments. Inside the EBU, two 4-port micro USB hubs are used to connect all internal components and to add two additional external USB ports at the back for additional devices. In this case, they serve to control syringe pumps automating the exchange of fluids in the flowcell. The internal components comprise a PowerDAC, a temperature measurement device, an impedimetric device and their supporting electronic components.

2.2.1 PowerDAC This device is essentially a precisely controlled dual channel voltage source with each channel capable of delivering up to 50 Watt in power (**Figure 5**). Connected to the power resistors inside heating elements it can be used as a controllable heat source. All active components are connected through an I²C-bus. The FT232B-SC18IM700 chip combination enables USB-communication with these components. The maximum voltage can be set to 5, 10, 25 or 50 V for each channel separately. The supply voltage of the PowerDAC needs to be at least 10 % higher than the highest selected maximum voltage.

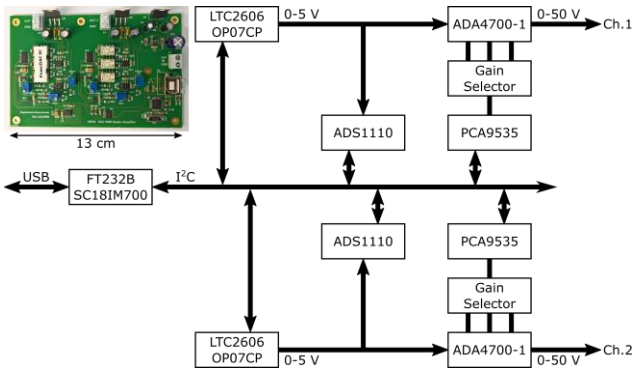

Figure 5 Schematic representation of the main components and interconnections of the PowerDAC device. (inset: Photograph with scale bar.)

The requested output voltage is achieved using a 2-stage process: In the first step, a digital to analogue (D/A) converter (LTC2606) combined with an operational amplifier (OP07CP) produces a voltage in the range 0 – 5 V. Finally, a second operational amplifier (ADA4700-1) increases this

voltage to the user-requested value. A set of three relays (G6K-2FY) controlled by a general purpose I/O-chip (PCA9535) determine the amplification factor in this second stage. Choices are 1 ×, 2 ×, 5 × and 10 × corresponding to the maximum voltages mentioned above. This flexibility in setting the maximum output voltage enables use of this device in low power applications where the maximum power delivered to the system needs to be restricted. Another advantage of using a 2-stage process is the possibility to monitor the actual output voltage during the measurements. To this end, an analogue to digital (A/D) converter (ADS1110) was placed between both stages.

2.2.2 Temperature Measurements For this purpose the National Instruments NI-9212 thermocouple card was selected. It offers 8 channel-to-channel isolated thermocouple inputs, cold-junction compensation and fast readouts of all channels simultaneously. Type K is the most common general-purpose thermocouple. It is inexpensive and its temperature range (0 °C to 1100 °C) and sensitivity (± 0.15 at 37 °C) are more than sufficient as the relevant temperature for biosensor measurements ranges from room temperature up to the denaturation temperature of DNA at around 90 °C. Thermocouples of type K with a diameter of 500 µm were purchased from TC Direct (The Netherlands).

2.2.3 Dual Reference Organic Impedimetric Device (DROID) Similarly to the PowerDAC, all the active components are interconnected via an I²C-bus and the FT232B-SC18IM700 chip combination enables USB-communication. However, unlike the PowerDAC, this device is completely USB-powered just as the NI-9212 mentioned in section 2.2.2. **Figure 6** shows a schematic representation of its main components: The core component is the AD5933 impedance analyser, which has already proven itself in custom impedimetric designs [25, 26]. Its output voltage can be set to four distinct levels (200 mV, 400 mV, 1.0 V and 2.0 V). For biological (organic) samples, the voltage between the sample and the counter-electrode should not exceed 70 mV [27]. Therefore, an adjustable voltage divider was added at the V_{out}-pin to reduce the output from 2 V to 65 mV. This allows lower settings to be programmatically enabled in case of very sensitive biological samples. Using its internal oscillator, the AD5933 has a frequency measurement range between 1 kHz and 100 kHz. To extend the lower limit to 10 Hz an external oscillator (DS1077) was added to the system.

For calibration purposes, a set of ten resistors ranging between 39 Ω and 3.9 MΩ were added to the device. During calibration, the phase-shift and impedance for the requested measurement frequencies is individually measured for each of these resistors and stored in a calibration file to be used during the actual biosensing measurements. To select the appropriate feedback-, measurement- and/or calibration channel, two general purpose I/O-chips (PCA9535) drive twenty-four relays (**inset Figure 6**). The LabView software calculates the phase-shift and impedance amplitudes from the real and imaginary values it receives from the AD5933 and adjusts these using the calibration data.

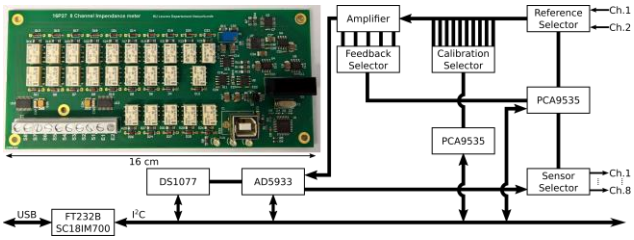

Figure 6 Schematic representation of the main components and interconnections of the DROID device. (inset: Photograph with scale bar.)

2.3 Final assembly The basic system consists of the DISC, the EBU and a computer running the measurement software. Optionally, any kind of USB-connectable liquid pumping system such as peristaltic or syringe-driven pumps can be attached to the EBU to simplify connections.

3 Device characterization Several control experiments were performed to determine the main device characteristics of the DISC. Based on previous experience the same PID parameters were used for both temperature controllers (P = 1, I = 8, D = 0). As can be seen from the heater profile T_H in **Figure 8** (Paragraph 4) there was no need for further optimization of these parameters, so they remained unchanged for all subsequent experiments. Furthermore, all measurements were carried out under no-flow conditions of the liquid inside the flowcell.

3.1 Materials Chips measuring 10 × 10 mm² were cut from a 0.5 mm thick aluminium sheet (Brico N.V., Leuven, Belgium). Polystyrene (M_w = 932 kDa), and anhydrous toluene (99.8 %) were purchased from Sigma-Aldrich (Diegem, Belgium).

3.2 Sensor chips Smooth aluminium substrates were covered with a thin polystyrene layer. Compared to gold-coated chips, aluminium chips are low-cost while having a similarly high electrical and thermal conductivity. They are also natively covered with a thin protective oxide layer that is stable at neutral pH values [28, 29]. Moreover, they have been tested before using polymers as a model system for biological layers and/or as an adhesive layer to attach MIPs [13-15]. To manufacture these chips, 8 mg of polystyrene was dissolved in 5 ml toluene. This solution was then left to cure while stirring at 80 °C under nitrogen atmosphere for 60 minutes before spin coating it onto the aluminium substrates (60 s at 3000 rpm). Finally, the substrates were stored at 80 °C under nitrogen atmosphere for 18 hours to completely cure the polystyrene. A layer thickness of 91 ± 7 nm was measured using an Agilent 5500 AFM system with NCSTR probes (spring constant 7.4 N/m, resonant frequency 160 kHz, tip radius of curvature < 7 nm) pur-

chased from NanoAndMore GmBH, Germany for morphological imaging in intermittent contact (AAC) mode. The AFM topography images were levelled, line-corrected and analysed (height profiles) using Gwyddion, a free and open-source SPM (scanning probe microscopy) data visualization and analysis program [30].

3.3 Heating characteristics After installing two identical sensor chips, the flowcell of the system was filled with a 1 × PBS solution. This PBS solution was chosen because it has similar salt concentrations, conductivity and pH value as typical biological samples like blood plasma. A stepped temperature profile for the heater elements was programmed into the system (25 °C, 30 °C, 35 °C, 37 °C, 40 °C and 50 °C) with each step lasting 2 hours. All temperatures and voltages were calculated by averaging the measurement over a 10-minute period starting 90 minutes after the start of each step. The required power P was calculated using **Equation 1** with R the resistance of one heater element and V the voltage applied to the respective heater elements.

$$P = \frac{V^2_{\text{heater bottom}} + V^2_{\text{heater top}}}{R} \qquad \textbf{(1)}$$

The results of these experiments were used to determine the temperature profile of the liquid inside the flowcell as well as the correlation between the temperature of the two heating elements and the resulting temperature inside the flowcell.

3.4 Impedance characteristics Similarly to the experiments performed to study the heating characteristics two identical sensor chips were installed and the flowcell filled with a 1 × PBS solution. Using **Equation 2**, which will be discussed in more detail in section 4, a stepped temperature profile was calculated and programmed into the system to set and stabilize the temperature of the liquid inside the flowcell at specific values (25 °C, 30 °C, 35 °C, 37 °C, 40 °C, 45 °C and 50 °C). Each step lasted 1 hour, during which the impedance measurement channels were disconnected from the EBU after 45 minutes and connected to a high-resolution dielectric spectrometer (Novocontrol, Alpha analyser). After 2 measurement cycles the DISC was reconnected to the EBU. Impedance measurements were performed in the frequency range 10 Hz to 100 kHz with 10 logarithmically equidistant points per decade. For both devices the results were averaged over three measurement cycles and the final results were then compared.

4 Results & Discussion The results displayed in **Figure 7** show a clear linear correlation between the temperature of the heating elements and temperature of the liquid inside the flowcell (**Equation 2**). In the equation, the heater (T_H) and flowcell temperature (T_C) are in Kelvin units as opposed to °C units in the figure.

$$T_H = 1.22 \cdot T_C - 66.32\ \text{K} \qquad (R^2 = 0.999) \qquad \textbf{(2)}$$

Based on this equation a temperature profile for the heater elements can be calculated to precisely control the liquid temperature inside the flowcell. **Equation 3** was constructed to fit the power values in **Figure 7.** The linear contribution is related to heat conduction and convection while the 4th order contribution relates to heat loss through radiation according to the law of Stefan-Boltzmann [31]. The small correction factor is presumably necessary because the aluminium enclosure of the DISC device, see **Figure 4**, acts as a radiation shield. The flowcell temperature (T_C) and ambient temperature (T_A) are in Kelvin units.

$$P = 0.037\frac{\text{W}}{\text{K}} \cdot (T_C - T_A) + 1.7 \cdot 10^{-9}\ \frac{\text{W}}{\text{K}^4} \cdot (T_C^4 - T_A^4) - 0.56\ \text{W}$$
$$(R^2 = 0.997) \qquad \textbf{(3)}$$

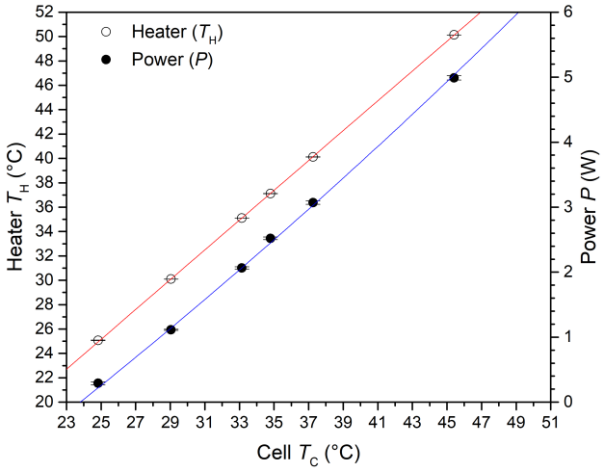

Figure 7 Required heater temperature (open circles) and power (closed circles) as a function of the chosen liquid temperature inside the flowcell. Linear fit (**Equation 2**) for the heater temperature (red line). Power fit based on **Equation 3** (blue line). Error bars were calculated by averaging measurements over a 10-minute period.

The measured data plotted in **Figure 8** show the response of the liquid temperature inside the flowcell when the temperature of the heater elements increases from 40 °C to 50 °C. The temperature oscillations of the heater elements (red line) are caused by the PID-controller trying to achieve the requested temperature as fast as possible. A fit algorithm based on an adapted version of Newton's law of cooling and heating (**Equation 4**) [32] was applied to the liquid temperature data (dotted line) resulting in a value of 0.0018 ± $3.8 \cdot 10^{-6}$ s^{-1} ($R^2 = 0.997$) for time constant $\bar{\alpha}$. In case the heater temperature would follow a step-profile the fit is expected to be perfect. However, during the first 10 minutes the heater temperature oscillates due to PID regulation. After this initial phase, the heater temperature stabilizes and changes in liquid temperature now fit perfectly with Newton's law of cooling and heating. The temperature of the liquid inside the flowcell stabilizes at its new level within 30 minutes.

$$T(t) = T_{\text{end}} - (T_{\text{end}} - T_{\text{start}}) \cdot \exp\{-\bar{\alpha} \cdot t\} \qquad \textbf{(4)}$$

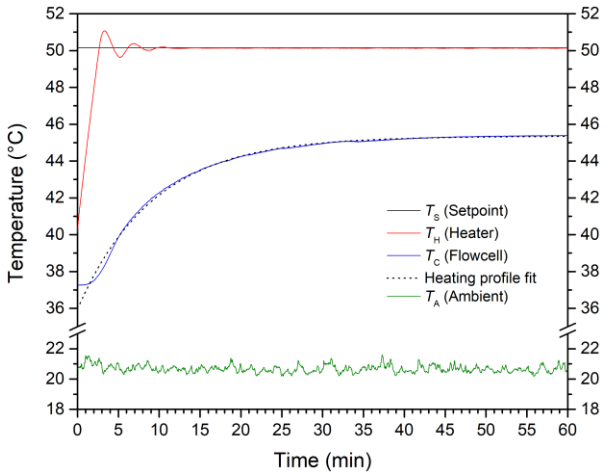

Figure 8 The left temperature scale refers to the heater temperature T_H (red line) while the right scale refers to the flowcell temperature T_C (blue line). Fluctuations in the ambient temperature T_A are presented as a green line. An adapted version of Newton's law of cooling and heating (**Equation 4**) was used to calculate a fit based on this profile (dotted line).

4.1 Validation of the impedance analyser As an example, **Figure 9** shows the impedance measurement results for both the Novocontrol and the DISC/EBU when the liquid temperature was stabilized at 30 °C. For both devices error bars were calculated by averaging three consecutive measurements. Comparing the results from both devices confirms that in the chosen frequency range the accuracy of the DISC/EBU is just as good as an established, high-end commercial instrument. Only at very low frequencies (around 10 Hz) a significant difference can be seen. However, at those frequencies the device operates beyond the frequency limits of the AD5933 impedance analyser chip. Comparing the impedance measurements results yielded a similar agreement between both instruments for the other liquid temperatures tested (25 °C, 30 °C, 35 °C, 37 °C, 40 °C, 45 °C and 50 °C). Moreover, as expected a decreasing trend can be seen for the impedance amplitude with rising liquid temperatures.

Figure 10 shows the impedance phase angle measurement results for both the Novocontrol and the DISC/EBU after the liquid temperature was stabilized at 30 °C. The underlying dataset is the same one that was used for **Figure 9**. At frequencies below 300 Hz both devices become less accurate. Considering the entire frequency range, the results for both devices are similar in the 1000 Hz to 10000 Hz range. Therefore, the DROID impedance analyser inside the EBU can provide a good indication of the phase angle during impedance measurements when necessary.

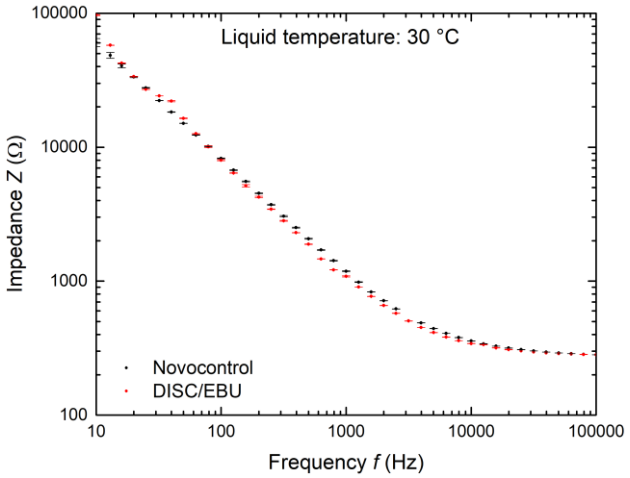

Figure 9 Comparison of the impedance amplitude measurement results between the DISC/EBU (red circles) and the Novocontrol instrument (black circles).

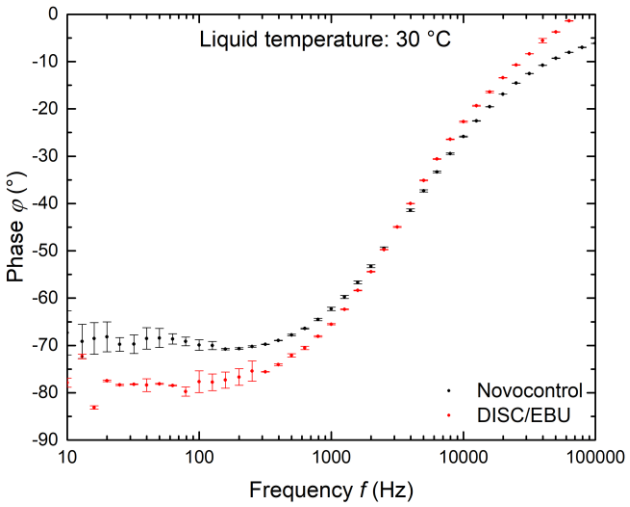

Figure 10 Comparison of the impedance phase angle measurement results between the DISC/EBU (red circles) and the Novocontrol instrument (black circles).

4.2 Cell constant determination Measurement cells in impedance spectroscopy are also characterized by their cell constant *c*, which is a measure of the ratio between the inter-electrode distance and the active surface area of the electrodes. Measurements with low conductivity require a low cell constant, while high conductivity measurements require a high cell constant [33]. Using the equivalent circuit shown in **Figure 11**, the Novocontrol measurement data from **Figure 9** were fitted and the obtained fitting parameters are summarized in **Table 1**.

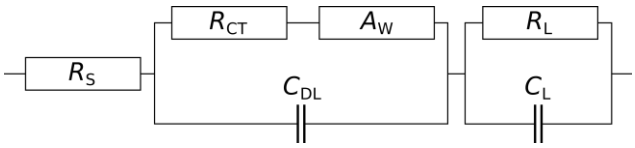

Figure 11 The equivalent circuit used for fitting the impedance data. From left to right respectively, the device resistance (R_S), the interface model (charge-transfer resistance (R_{CT}), double-layer capacitance (C_{DL}) and Warburg element (A_W)) and the liquid model (liquid resistance (R_L) and liquid capacitance (C_L)).

The liquid resistance (R_L) was calculated to be 109 Ohm based on the conductivity of the 1 × PBS solution (γ_{PBS}) that was measured at 1.2 S/m using a Mettler Toledo S230 conductivity meter. Using **Equation 5**, the cell constant was calculated to be 130.8 m^{-1}.

Table 1 Fitting results Novocontrol data with an equivalent circuit.

Parameter	Description	Value
R_S	Device resistance	248 Ohm
A_W	Warburg coefficient	344600 Ohm.$s^{-0.5}$
C_{DL}	Double layer capacitance	163 nF
R_{CT}	Charge-transfer resistance	209 µOhm
C_L	Liquid capacitance	214 nF
R_L	Liquid resistance	109 Ohm

$$\gamma_{PBS} = \frac{1}{R_L} \cdot c \qquad \text{or} \qquad c = \gamma_{PBS} \cdot R_L \qquad \textbf{(5)}$$

This value is a very good approximation: Based on the flowcell geometry and a distance between the electrodes of 5 mm a value of 147.5 m^{-1} was expected. This value was calculated using the average surface area of the chip (56.8 mm^2) and the gold wire (11.0 mm^2), resulting in an average electrode size of 33.9 mm^2.

5 Conclusion The aim of this work was to develop an easy to use device to perform simultaneous multi-channel impedance measurements on a single liquid sample. In its simplest form, it measures one bio-molecular target and one background reference. Using two 4-channels models any combination of reference and target sensors can be used up to a total of 8 channels. The heating characteristics of the system show that it is fast, liquid temperature stabilizes within 30 minutes after changing the setpoint temperature for the heater elements, and that it has a linear correlation between the temperature of the heater elements and the liquid inside the flowcell allowing precise control of all temperatures. Moreover, the performance of the home-made DROID impedance analyser was validated against a high-resolution dielectric spectrometer from Novocontrol. All these results clearly demonstrate the promising potential of the DISC/EBU system. More proof-of-concept measurements are ongoing to determine the performance of this novel and innovative device in more detail in real bioanalytical applications.

Acknowledgements Financial support by the Research Foundation Flanders FWO, Project G.0B25.14N "Monitoring of gut functions and inflammation processes with biomimetic sensors based on molecularly imprinted polymers", the KULeuven C1 project, C14/15/067 "Smart Cellular Scaffolds", the KULeuven FLOF scholarship of Peter Cornelis and the ERASMUS travel fellowships of the European Union of Max Brand and Isabelle Thomas are gratefully acknowledged. Scientific advice by Heiko Iken and Prof. Dr.-Ing. Michael Josef Schöning from the Aachen University of Applied Sciences (FH Aachen), technical support by Werner Neefs and Valentijn Tuts (both in KULeuven) and AFM imaging by Dr. Olivier Deschaume (KULeuven) are greatly appreciated.

References

[1] E. B. Bahadir and M. K. Sezgintürk, Artificial Cells Nanomedicine and Biotechnology **44 (1)**, 248-262 (2016).
[2] M. I. Prodromidis, Electrochimica Acta **55 (14)**, 4227-4233 (2010).
[3] J. S. Daniels and N. Pourmand, Electroanalysis **19 (12)**, 1239-1257 (2007).
[4] E. Katz and I. Willner, Electroanal. **15 (11)**, 913-947 (2003).
[5] M. Riedel, J. Kartchemnik, M. J. Schöning, and F. Lisdat, Anal. Chem. **86**, 7867-7874 (2014).
[6] M. S. Murib, B. van Grinsven, L. Grieten, S. D. Janssens, V. Vermeeren, K. Eersels, J. Broeders, M. Ameloot, L. Michiels, W. De Ceuninck, K. Haenen, M. J. Schöning, and P. Wagner, Phys. Status Solidi A. **210 (5)**, 911-917 (2013).
[7] B. van Grinsven, N. Vanden Bon, L. Grieten, M. Murib, S. D. Janssens, K. Haenen, E. Schneider, S. Ingebrandt, M. J. Schöning, V. Vermeeren, M. Ameloot, L. Michiels, R. Thoelen, W. De Ceuninck, and P. Wagner, Lab Chip **11 (9)**, 1656-1663 (2011).
[8] J. Posseckardt, C. Schirmer, A. Kick, K. Rebatschek, T. Lamz, and M. Mertig, Sensors and Actuators B-Chemical **255**, 3417-3424 (2018).
[9] A. Kleppisius, A. Kick, and M. Mertig, Phys. Status Solidi A. **214 (9)**, 1600921 (2017).
[10] V. Vermeeren, L. Grieten, N. Vanden Bon, N. Bijnens, S. Wenmackers, S. D. Janssens, K. Haenen, P. Wagner and L. Michiels, Sensors and Actuators B-Chemical **157 (1)**, 130-138 (2011).
[11] D. T. Tran, V. Vermeeren, L. Grieten, S. Wenmackers, P. Wagner, J. Pollet, K. P. P. Janssen, L. Michiels, and J. Lammertyn, Biosensors & Bioelectronics **26 (6)**, 2987-2993 (2011).
[12] R. E. Ionescu, C. Gondran, L. Bouffier, N. Jaffresic-Renault, C. Martelet, and S. Cosnier, Electrochimica Acta **55 (21)**, 6228-6232 (2010).
[13] M. Peeters, F. J. Troost, R. H. G. Mingels, T. Welsch, B. van Grinsven, T. Vranken, S. Ingebrandt, R. Thoelen, T. J. Cleij, and P. Wagner, Anal. Chem. **85**, 1475-1483 (2013).
[14] M. Peeters, F. J. Troost, B. van Grinsven, F. Horemans, J. Alenus, M. S. Murib, D. Keszthelyi, A. Ethirajan, R. Thoelen, T. J. Cleij, and P. Wagner, Sensor and Actuators B -Chemical **171**, 602-610 (2012).

[15] R. Thoelen, R. Vansweevelt, J. Duchateau, F. Horemans, J. D'Haen, L. Lutsen, D. Vanderzande, M. Ameloot, M. vandeVen, T. J. Cleij, and P. Wagner, Biosensors & Bioelectronics **23 (6)**, 913-918 (2008).
[16] K. Norman, N. Stobaus, M. Pirlich, and A. Bosy-Westphal, Clinical Nutrition **31 (6)**, 854-861 (2012).
[17] M. Y. Jaffrin and H. Morel, Medical Engineering & Physics **30 (10)**, 1257-1269 (2008).
[18] J. R. Mager, S. D. Sibley, T. R. Beckman, T. A. Kellogg, and C. P. Earthman, Clinical Nutrition **27 (6)**, 832-841 (2008).
[19] L. Lehane and J. Olley, Int. J. Food Microbiol **58 (1-2)**, 1-37 (2000).
[20] L. F. Bjeldanes, D. E. Schutz, and M. M. Morris, Food Cosmet. Toxicol. **16 (2)**, 157-159 (1978).
[21] T. P. Nguya, T. Van Phi, D. T. N. Tram, K. Eersels, P. Wagner, and T. T. N. Lien, Sensors and Actuators B-Chemical **246**, 461-470 (2017).
[22] A. Bouafsoun, S. Helali, S. Mebarek, C. Zeiller, A. F. Prigent, A. Othmane, A. Kerkeni, N. Jaffrezic-Renault, and L. Ponsonnet, Bioelectrochemistry **70 (2)**, 401-407 (2007).
[23] W. Chen, W. Zhu, O. K. Tan, and X. F. Chen, J. Appl. Phys. **108**, 34101 (2010); doi: 10.1063/1.3457217
[24] D. M. Zhou, E.T Mcadams, A. Lackermeier, and J. G. Jones in: Proceedings of the 16th Annual International Conference of the IEEE Engineering in Medicine and Biology Society - Engineering Advances: New Opportunities for Biomedical Engineers, Pts 1&2, 1994, pp. 832-833.
[25] J. Broeders, S. Duchateau, B. Van Grinsven, W. Vanaken, M. Peeters, T. Cleij, R. Thoelen, P. Wagner, and W. De Ceuninck, Phys. Status Solidi A. **208 (6)**, 1357-1363 (2011).
[26] B. van Grinsven, T. Vandenryt, S. Duchateau, A. Gaulke, L. Grieten, R. Thoelen, S. Ingebrandt, W. De Ceuninck, and P. Wagner, Phys. Status Solidi A **207 (4)**, 919-923 (2010).
[27] S. H. Wright, Adv. Physiol. Educ. **28 (4)**, 139-142 (2004).
[28] J. Evertsson, F. Bertram, F. Zhang, L. Rullik, L. R. Merte, M. Shipilin, M. Solderno, S. Ahmadi, N. Vinogradov, F. Carla, J. Weissenrieder, M. Gothelid, J. Pan, A. Mikkelsen, J. O. Nilsson, and E. Lundgren, Applied Surface Science **349**, 826-832 (2015).
[29] L. P. H. Jeurgens, W. G. Sloof, F. D. Tichelaar, and E. J. Mittermeijer, Thin Solid Films **418 (2)**, 89-101 (2002).
[30] D. Nečas and P. Klapetek, Cent. Eur. J. Phys. **10 (1)**, 181-188 (2012).
[31] A. De Vos, Journal of Physics and Chemistry of Solids **49 (6)**, 725-730 (1988).
[32] M. Gockenbach and K. Schmidtke, Involve Mathematical Journal **2 (4)**, 439-450 (2009).
[33] Metrohm Application Bulletin 102/2 e: Conductometry, https://www.metrohm.com/en/applications/#, Retrieved on November 9, 2017.